Journal of Applied Fluid Mechanics, Vol. 13, No. 1, pp. 119-132, 2020.
Available online at www.jafmonline.net, ISSN 1735-3572, EISSN 1735-3645.
DOI: 10.29252/jafm.13.01.29896

Parameter and Design Analysis for Gasoline Direct Injection Injector using CFD and Design of Experiments

B. Biçer[1] and A. Yurtkuran[†2]

[1] *Robert Bosch A. S. BTSO Organized Industrial Zone, Eflatun Cad. No 9. Bursa, Turkey*
[2] *Department of Industrial Engineering, Uludag University, Bursa, Turkey*

†*Corresponding Author Email: alkin@uludag.edu.tr*

(Received December 7, 2018; accepted May 26, 2019)

ABSTRACT

Numerical modeling of internal nozzle flow can be regarded as an essential investigation in the field of gasoline direct injection system of combustion engines since it is directly connected with fuel spray atomization and subsequently efficiency of exhaust gas emission. Internal nozzle flow can be changed and formed according to several parameters such as; system pressure, chosen fuel type, the orientation of spray holes according to injector axis, conicity of spray holes and distribution of spray holes on valve-seat, etc. The changes in these parameters also affect the formation of cavitation inside of whole domain, spray angle and create wall-wetting on the spray hole surfaces. The present work investigates the parameter and design analysis in the valve-seat region of direct gasoline injection (GDI) injector using Computational Fluid Dynamics (CFD) and Design of Experiments (DOE). CFD is employed to study the behaviors of internal flow inside the valve-seat region according to several design parameters, whereas a mixed-level factorial design is used to test the significance of the effects on the response variables. In conclusion, the effects of the most significant factors on response parameters as amount of vapor formation, spray (Tau) angle, and pre-hole wall wetting are determined for further efficient design.

Keywords: CFD; In-nozzle simulation; Cavitation; Gasoline direct injection; Design of experiments.

NOMENCLATURE

DF	fuel types
DP	system pressure
f_v	void fraction
F	empirical calibration coefficient
N_B	number of bubbles per unit volume
P	surrounding pressure around of bubble
P	thermodynamic pressure
P_v	pressure in the bubble
RANS	Reynolds-Averaged-Navier-Stokes
RP	Rayleigh-Plesset
R_B	bubble radius
R_{nuc}	nucleation site radius
S_c	source term for the mass transfer of condensation
S_e	bubble growth
S_e	source term for the mass transfer of evaporation
TauOut	spray angle at out plane
U_j	mixture velocity
VSW1	pre-hole wall wetting
VVF	amount of vapor creation
μ_{eff}	effective viscosity
ρ_m	mixture density
σ	surface tension

1. INTRODUCTION

Nowadays, the growing apprehension over environmental pollution caused by cars and heavy vehicles bring new stringent emission regulations, which leads to further improvement of combustion process of both in gasoline and diesel engines (WHO, 2003; Xu *et al.*, 2016). Further developments are directly connected with fuel spray atomization inside the gasoline engine since it decreases the exhaust gas emissions and increases the efficiency. Previous works show that characteristics of spray inside the combustion chamber are strongly affected by cavitation

phenomena, which occurs inside the injector nozzle under high injection pressure (Bicer, 2015; Chaves *et al.*, 1995; Hiroyasu, 1991; Sou *et al.*, 2007). Although cavitation can create a negative impact on pumps, valves, and injectors, such as erosion damage, it can also improve the process of atomization by increasing the spray angle and homogenous distribution inside combustion chamber

Previous studies and investigations related to internal flow inside injector showed that cavitation plays a significant role in order to develop fuel spray and further optimize the combustion processes. (Biçer and Sou, 2016; Bicer *et al.*, 2013). The main reason for cavitation formation is the sudden pressure drop below the saturation pressure of liquid fuel, which can be created by acoustic or hydraulic factors. Acoustic cavitation is formed from pressure difference since the pressure wave propagates through the liquid flow such can be observed like in high-pressure injection engines, transmission and traction control systems (Ferrari, 2010). Hydraulic cavitation is produced during the pressure reduction due to the hydrodynamic motion of fluid flow such as boundary layer separation from the wall of the orifice inlet (He *et al.*, 2016). This separation results in an abrupt change in the flow passage and direction of internal velocity flow and leads to flow contraction, causing to decrease of static pressure below the vapor pressure of the fluid. In this work, hydraulic cavitation is considered.

An experiment is a series of systematic tests, which attempt to find the factors, which have the largest effect on a response variable (Montgomery, 2017). Traditionally, the effect of factors on the response variable has been tested by altering the levels of one-variable-at-a-time (OVAT) while the other factors are held constant. However, this approach disregards the information about possible factor interactions. The design of experiment (DOE) is a popular approach to analyze the effects of multiple design parameters as inputs on the output parameters as response variables. By DOE, one can investigate not only the main effects of the inputs but also interaction effects of the main factors (Antony, 2014).

In literature, various DOE studies combined with CFD simulations have been proposed. To mention a few, Jin and Untaroiu (2018) presented a CFD-DOE study to investigate the effects of different geometrical properties on the overall performance of a hole-pattern annular gas seal. Yoon and Lee (2018) analyzed the effects of different parameters for the design of hovering thrust of a quad-rotor air vehicle using CFD simulations and DOE. Kear *et al.*, (2016) presented an approach for the optimal design of a vertical axis wind turbine using DOE and the results of the CFD simulations. Chen *et al.* (2015) investigate and formulate the correlation of the fuel spray sauter mean diameter using factors such as viscosity, fuel injection pressure, and air-blast pressure. They implemented a response surface methodology to optimize the design parameters. He and Dass (2018) investigate the main and interaction effects of design parameters on the performance of electrostatic precipitators through a full factorial two-level DOE. Chapela *et al.* (2018) studied the deposition of undesirable matter of the surfaces in biomass combustion. In this study, authors developed a model using CFD and the effects of several operational parameters were tested through a robust central composite design based on a latin hyber-cube sampling. Lee *et al.* (2018) implemented CFD analysis with a response surface model in order to evaluate the factors influencing the drag coefficient of a sedan in the double-deck tunnel system. In another study, researchers employed CFD analysis and Taguchi DOE to optimize the aerodynamic performance of a typical three-bladed vertical-axis wind turbine (Wang *et al.*, 2018). Zhang *et al.* (2017) used CFD simulations and factorial designs to investigate the effect of the impeller on the sinking and floating performance of suspended particles in a stirred tank. They used three different 23 full factorial designs. In the study by Yang *et al.* (2017), CFD simulations and response surface designs were used to optimize the membrane bioreactor hydrodynamics for cake layer fouling control.

The presented study aims to investigate the parameter and design analysis in the valve-seat region of gasoline direct injection (GDI) injector using CFD and DOE. For this purpose, a mixed-level factorial design is created using different physical (injection pressure & different fuels) and geometric design parameters such as I-angle, conicity, and pitch circle diameter, which intensively affect the internal flow inside the injector. The effects of aforementioned design parameters are investigated using CFD simulations and DOE analysis regarding atomization and emission related response variables such as spray (Tau) angle (TauOut), amount of vapor creation (cavitation) inside computation domain (VVF) and Pre-hole wall wetting (VSW1). In other words, a full mixed-level factorial design is generated, then the results of the response variable are obtained from CFD simulations for each design point, and a DOE analysis is conducted to provide insights into the effects of these design parameters on the response variables. In other words, the physical and geometric parameters were optimized in accordance to a mixed 2 and 3 level full factorial design, where the effect of injection pressure, fuel type, conicity, and pitch circle diameter as two levels of factors and I-angle as three levels of factor were investigated. This paper creates an important outlook on the design phase of valve-seat to understand effects of several input parameters effects on internal flow, which also subsequently affects the efficiency of atomization and emission.

The rest of this paper is organized as follows. In Section 2, the numerical methodology and cavitation models are given. Input parameters and response variables are described in Section 3. Section 4 is dedicated to results of DOE studies. Finally, Section 5 summarises the conclusions and directions for future research.

2. COMPUTATIONAL FLUID DYNAMICS

This section describes the numerical methodology and cavitation models, which are covered in this study.

2.1 Numerical Methodology

It is really important to precisely define vapor and liquid fractions and the resulting change in the mixture fluid properties in the numerical modeling of internal flow inside injector (Bicer, 2015). In the present work, Reynolds-Averaged-Navier-Stokes (RANS) equations for homogeneous multiphase mixture are used for simulation methodology. This model presumes that the liquid and vapor phase are perfectly mixed in homogeneous equilibrium which means that velocity, temperature, turbulence field, etc. are equal for both phases.

The continuity and momentum equations for the two-phase (single) fluid mixture flow are given as follows (Gong and Baar, 2017):

$$\frac{\partial p_m}{\partial t}+\frac{\partial (p_m U_j)}{\partial x_j}=0 \tag{1}$$

$$\frac{\partial (\rho_m U_j)}{\partial t}+\frac{\partial (\rho_m U_i U_j)}{\partial x_j}=-\frac{\partial P}{\partial x_i}+\frac{\partial}{\partial x_j}\left[\mu_{eff}\left(\frac{\partial U_i}{\partial x_j}\right)+\left(\frac{\partial U_j}{\partial x_i}\right)\right] \tag{2}$$

where $P, \rho_m, \mu_{eff}, x_i=(x,y,z)$ and $U_i=(U,V,W)$ are thermodynamic pressure, mixture density, effective viscosity, Cartesian coordinates, and mixture flow velocity components, respectively. The simulation covers the following assumptions:

- Ansys-CFX tool is used for in-nozzle simulations (ANSYS, 2015).
- Thermal effects are ignored.
- The two-phase mixture flow is incompressible where mixture density (ρ_m) and mixture viscosity (μ_m) are taken into account. They are expressed using Eqs. (3) and (4) as below:

$$\rho_m=\alpha\rho_l+(1-\alpha)\rho_v \tag{3}$$

$$\mu_m=\alpha\mu_l+(1-\alpha)\mu_v \tag{4}$$

where suffixes l and v denote liquid and vapor phases, and α is the volume fraction. As explained above μ_{eff} is effective viscosity and given by:

$$\mu_{eff}=\mu_m+\mu_t \tag{5}$$

where, μ_t denotes the turbulence viscosity and turbulence effects are represented using the k-ωSST model which is developed by Menter (1994). This model includes the blending function between the k-ω model near the walls and the k-ε model in the outer region. Further, the definition of the turbulent viscosity is modified to account the transport of the turbulent shear stress. These features make the kω-SST model more accurate and reliable for industrial applications. In addition to these features, with the help of previous experiences (Bicer, 2015; Biçer and Sou, 2016) and related literature (Bicer and Sou, 2015; Pierrat *et al.*, 2008; Zhang *et al.*, 2013), the kω-SST model is chosen for the modeling of turbulence in this paper.

2.2 Cavitation Model

The transport equation based on the liquid volume fraction is introduced to close the system instead of the energy equation as follows:

$$\frac{\partial \alpha\rho_l}{\partial t}+\frac{\partial (\rho_l \alpha U_j)}{\partial x_j}=S_c+S_e \tag{6}$$

where U_j, S_c, and S_e are the mixture velocity, source terms for the mass transfer of condensation and evaporation, respectively.

Rayleigh-Plesset (RP) model is used for the representation of mass transfer due to cavitation (Prosperetti, 1982). This model assumes that the change of bubble size is driven by the difference in vapor pressure across the bubble surface and displays the basic representation of bubble formation (evaporation) and collapse (condensation). RP model equation is described in Eq. (7).

$$R_B\frac{d^2R_B}{dt^2}+\frac{3}{2}\left(\frac{dR_B}{dt}\right)^2+\frac{2\sigma}{\rho_l R_B}=\frac{P_v-P}{\rho_l} \tag{7}$$

where R_B, P_v, P, and σ are bubble radius, the pressure in the bubble (assumed to be equal to liquid vapor pressure at the liquid temperature), surrounding pressure around of bubble and surface tension, respectively. Simplified RP equation is given by neglecting the surface tension and second-order terms as follows:

$$\frac{dR_B}{dt}=\sqrt{\frac{2}{3}\frac{P_v-P}{\rho_l}} \tag{8}$$

According to the pressure change in Eq. (7), vapor bubbles grow and collapse. The rate change in bubble volume (v_B) is calculated as follows (Gong and Baar 2017):

$$\frac{dv_B}{dt}=\frac{d}{dt}\left(\frac{4}{3}\Pi R_B^3\right)=4\Pi R_B^2\sqrt{\frac{2}{3}\frac{P_v-P}{\rho_l}} \tag{9}$$

If N_B shows the number of bubbles per unit volume, the void fraction (f_v) can be stated as:

$$f_V=V_B N_B=\frac{4}{3}\Pi R_B^3 N_B \tag{10}$$

The net mass transfer rate for evaporation, S_e (bubble growth) is given by:

$$S_e=N_B\frac{dm_B}{dt}=\frac{3f_V\rho_V}{R_B}\sqrt{\frac{2}{3}\frac{|P_v-P|}{\rho_l}} \tag{11}$$

Equation (11) can be generalized in order to satisfy the bubble collapse process (condensation, S_c) as follows:

$$S_C=F\frac{3f_V\rho_V}{R_B}\sqrt{\frac{2}{3}\frac{|P_v-P|}{\rho_l}}sign(P_v-P) \tag{12}$$

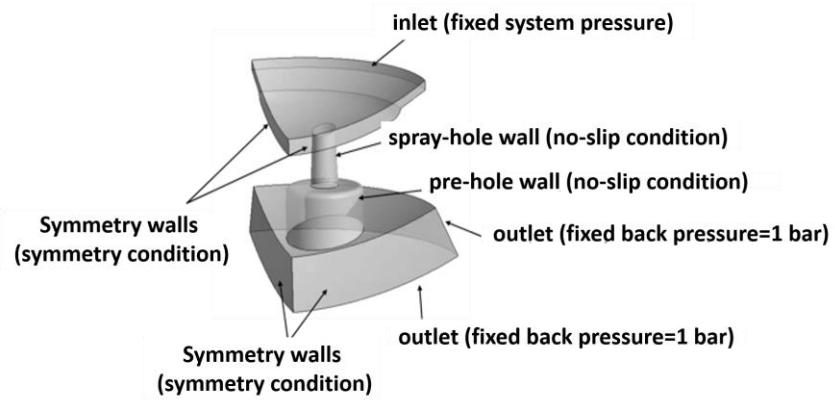

Fig. 1. 3-D computational geometry and boundary conditions.

where F denotes the empirical calibration coefficient.

In Ansys-CFX solver for the modeling purpose, the nucleation site radius (R_{nuc}) is used instead of the bubble radius (R_B). The R_{nuc} should decrease since the vapor volume fraction increases due to less liquid. Additionally, void fraction is replaced by $f_{nuc}(1 - f_v)$ for evaporation model as follows:

$$S_e = F \frac{3 f_{nuc}(1-f_V)\rho_V}{R_{nuc}} \sqrt{\frac{2}{3}\frac{|P_v - P|}{\rho_1}} sign(P_v - P) \tag{13}$$

Then the final form of RP cavitation model in CFX is as follows:

If P ≤ Pv which means bubbles are growing for evaporation:

$$S_e = F_{vap} \frac{3 f_{nuc}(1-f_V)\rho_V}{R_{nuc}} \sqrt{\frac{2}{3}\frac{P_v - P}{\rho_1}} \tag{14}$$

If P≥Pv, which means that bubbles are collapsing for condensation:

$$S_C = F_{cond} \frac{3 f_V \rho_V}{R_{nuc}} \sqrt{\frac{2}{3}\frac{P_v - P}{\rho_1}} \tag{15}$$

Following default parameters are used during simulation in Ansys-CFX: $R_{nuc} = 1\mu m$, $fnuc = 5E-4$, $Fvap = 50$, $Fcond = 0.01$.

2.3 Geometry and Boundary Conditions

In the present work, one-hole simplified geometry is used for calculations as shown in Fig. 1. Spray hole diameter is 143 µm, whereas pre-hole diameter is 450 µm. Applied boundary conditions are also displayed in Fig. 1. Ansys-workbench Design modular tool is used for geometry preparation.

2.4 Mesh Description and Calculations

Internal flow simulations are strongly affected by computational mesh, especially in the zones where high gradients in velocity are obtained. For that reason, a mesh independence study is carried out to verify the proper mesh using three different meshes whose properties are indicated in Table 1.

Table 1 Properties of different meshes

	Course mesh	Middle mesh	Fine mesh
Total mesh number (million)	1.25	1.8	2.3
CPU time (hours)	52	60	72
CPU number (parallel)	48	48	48

We have created uniform hexahedral structured meshes using Ansys-workbench mesh tool. Figure 2 shows the structured fine mesh with 2.3 million hexahedral cells. Table 2 displays comparison of measured and calculated mass flows. As can be seen in the results, course and middle meshes underestimate the mass flow, while the fine mesh almost good prediction when compared to measured flow rate. Since Bosch standard gives +/-6% limits during flow rate measurement, the fine mesh is chosen for all simulations.

Table 2 Comparison of mass flows

	Mass flow (g/s)	Deviation (%)
Measured	2.40	-
Course mesh	1.55	-35.42
Middle mesh	1.93	-19.59
Fine mesh	2.28	-5.00

Bosch High-Performance Computing system with 48 CPU is used for each calculation and each calculation takes around 72 hours. All simulations are first run 300 steps in the steady-state mode to develop initial flow fields, and then 1100 steps are run in transient mode.

3. DOE BASED PARAMETER DESIGN

In this section the input parameters, response variables and corresponding DOE setup are summarized.

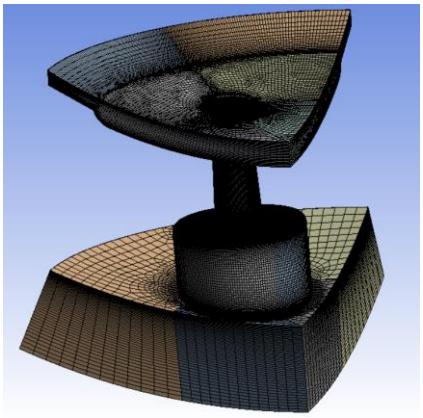

Fig. 2. 3-D computational grid.

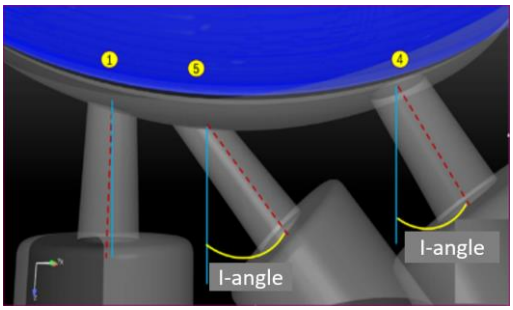

Fig. 3. I-angle orientations.

3.1 Input Parameters

Following physical and geometrical design parameters are used in DOE study:

- **System Pressure:** In GDI injector 250 bar and 350 bar system pressures are chosen as an input parameter.
- **Fuel type:** Several types of gasoline fuels are used in the field according to locations. In this work, the most complicated and problematic ethanol-based E30 and E85 blended gasoline fuels are chosen.
- **Temperature:** Since most of ethanol-based fuels work at 75ºC in the field, fuel temperature is taken as constant.
- **I-angle:** It corresponds to the orientation of each hole according to the injector line as indicated below in Fig. 3. Three different I angle values are chosen for investigation (low, medium, high)
- **Conicity:** An injector hole divided into two regions such as pre-hole and spray hole (See Fig. 4) for Bosch type GDI injector. Hole conicity is set to positive (Pos.) and negative (Neg.) as indicated in Fig. 5. Since conicity values are Bosch internal information, in this paper they will be represented as Pos. and Neg. conicity.
- **Pitch circle diameter:** It shows the diameter of holes' orientation on the valve-seat as indicated below Fig. 6. Since the pitch circle diameter values are Bosch internal information, here it is represented minimum and maximum in terms of dimension mm.

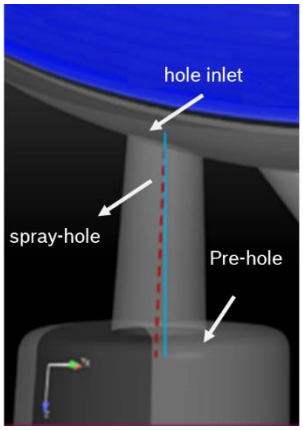

Fig. 4. Bosch hole representation.

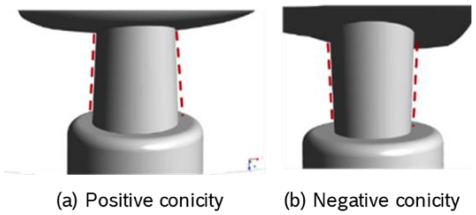

Fig. 5. Conicity representation.

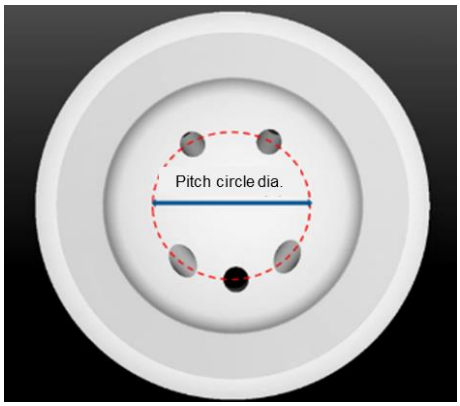

Fig. 6. Pitch circle diameter representation.

3.2 Response Variables

In this subsection, the response parameters are explained and the analytical effects of input parameters on corresponding response variables are discussed.

- **Spray (Tau) angle at out plane (TauOut):** It shows the angle of sprays as indicated in Fig. 7.
- **Amount of vapor creation (cavitation) inside the computation domain (VVF):** It is calculated as an average volume of created vapor amount during the transient simulation inside the whole domain.

Table 3 Input and Response Variables

Input parameters	Coded Label	Levels	# of levels	Response Variables		
System Pressure	DP	250 & 350 (bar)	2	VVF	VSW1	TauOut
Fuel type	DF	E30 & E85	2			
I-angle	IA	low & medium & high (º)	3			
Conicity	Conicity	Pos. & Neg. (º)	2			
Pitch Circle Diameter	PCD	Minimum & Maximum (mm)	2			

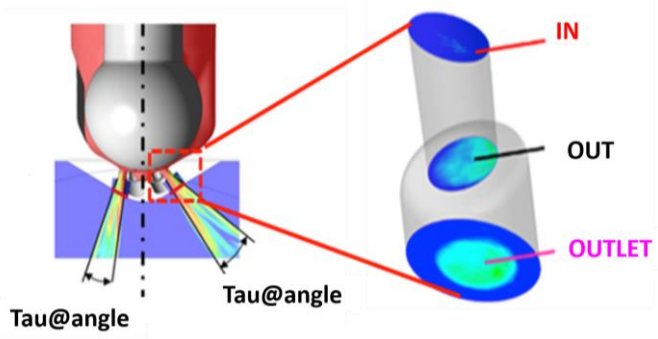

Fig. 7. Spray (Tau) angle and plane definitions (Henn, 2012).

- **Pre-hole wall wetting (VSW1):** this parameter represents the amount of liquid fuel on the pre-hole of the injector in terms of percentage.

All the above input and response variables, their levels, and values are summarized in Table 3. All defined respond variables are calculated from the transient CFD simulation based on Eq. (6), which shows volume fraction of fuel liquid. Volume fraction of fuel vapor is calculated as 1-α. Afterwards, transient average is taken to find exact values. Spray angle (TauOut) is the function of liquid velocity and volume fraction of liquid fuel. Amount of vapor creation (VVF) is calculated as volume of region, which occupied as vapor according to Eq. (6). To calculate the Pre-hole wall wetting (VSW1) fuel liquid fraction is taken as volume on the wall and then converted as percentage for each calculation.

Further, as can be seen from Table 3, for full factorial 2 and 3 levels design with one parameter in three levels and four parameters with two levels, 48 ($2^4 \times 3$) experiment points are generated, and simulation was carried out at each experiment point. Moreover, the response variables are also tabulated in Table 3. The DOE setup, factor levels and case numbers are given in Table 4.

4. RESULTS AND DISCUSSIONS

In this section, the results and discussions of corresponding experiments are given. For each response variable, the results are given in terms of ANOVA tables, Pareto charts of standardized effects, and main effect plots. The Pareto charts are used to compare the relative magnitude of both main and interaction effects. Further, the charts also show the reference line for the p-value, which is the %95 confidence level line. Moreover, the main effect plots display the means of response variable values for each level within a given input parameter. Last, the CFD results on selected cases are illustrated for each response variable.

4.1 Effects of Input Parameters on the Amount of Vapor Creation (VVF)

Main effects and the effects of two-way linear interactions on VVF are summarized in Table 5. The effects of the main and two level interactions that are depicted in bold are statistically significant ($p < 0.05$) in 95% confidence levels. In other words, the linear effects of DF, Conicity, PCD, the two-way interactions of DF * IA and DF * PCD, and the quadratic effect of IA on the response VVF are significant. Further, the Pareto chart of standardized effects on VVF is given in Fig. 8, where the effects are sorted from most to least significance and each bar is proportional to the standardized effect size. Figure 8 shows that the VVF is affected by aforementioned factors significantly. Further, the Pareto chart demonstrate that, DF is the most powerful factor affecting the VVF followed by Conicity, IA, DF * IA, PCD, and DF * PCD. Combining the results given in Table 5 and Fig. 8, VVF is significantly affected by DF, IA, Conicity, and PCD parameters.

Finally, in order to clearly illustrate the effects directions on VVF, main effects plots are figured in Fig. 9. As a result, one can say that better VVF values can be achieved by setting DF at E30, Conicity at Pos., PCD at Maximum and IA at High levels.

Table 4 Full factorial DOE experimental setup

Case	DP	DF	PCD	Conicity	IA
1	250	E30	Minimum	Pos.	Low
2	250	E30	Minimum	Pos.	Medium
3	250	E30	Minimum	Pos.	High
4	250	E30	Minimum	Neg.	Low
5	250	E30	Minimum	Neg.	Medium
6	250	E30	Minimum	Neg.	High
7	250	E30	Maximum	Pos.	Low
8	250	E30	Maximum	Pos.	Medium
9	250	E30	Maximum	Pos.	High
10	250	E30	Maximum	Neg.	Low
11	250	E30	Maximum	Neg.	Medium
12	250	E30	Maximum	Neg.	High
13	250	E85	Minimum	Pos.	Low
14	250	E85	Minimum	Pos.	Medium
15	250	E85	Minimum	Pos.	High
16	250	E85	Minimum	Neg.	Low
17	250	E85	Minimum	Neg.	Medium
18	250	E85	Minimum	Neg.	High
19	250	E85	Maximum	Pos.	Low
20	250	E85	Maximum	Pos.	Medium
21	250	E85	Maximum	Pos.	High
22	250	E85	Maximum	Neg.	Low
23	250	E85	Maximum	Neg.	Medium
24	250	E85	Maximum	Neg.	High
25	350	E30	Minimum	Pos.	Low
26	350	E30	Minimum	Pos.	Medium
27	350	E30	Minimum	Pos.	High
28	350	E30	Minimum	Neg.	Low
29	350	E30	Minimum	Neg.	Medium
30	350	E30	Minimum	Neg.	High
31	350	E30	Maximum	Pos.	Low
32	350	E30	Maximum	Pos.	Medium
33	350	E30	Maximum	Pos.	High
34	350	E30	Maximum	Neg.	Low
35	350	E30	Maximum	Neg.	Medium
36	350	E30	Maximum	Neg.	High
37	350	E85	Minimum	Pos.	Low
38	350	E85	Minimum	Pos.	Medium
39	350	E85	Minimum	Pos.	High
40	350	E85	Minimum	Neg.	Low
41	350	E85	Minimum	Neg.	Medium
42	350	E85	Minimum	Neg.	High
43	350	E85	Maximum	Pos.	Low
44	350	E85	Maximum	Pos.	Medium
45	350	E85	Maximum	Pos.	High
46	350	E85	Maximum	Neg.	Low
47	350	E85	Maximum	Neg.	Medium
48	350	E85	Maximum	Neg.	High

Table 5 ANOVA results for VVF

Source	Sum of Squares	Degree of freedom	Mean Square	F Value	*p*-value
DF(L)	10408.65	1	10408.65	339.6533	0.000000
DP(L)	24.92	1	24.92	0.8133	0.371395
Conicity(L)	2642.60	1	2642.60	86.2329	0.000000
IA(L)	110.35	1	110.35	3.6010	0.063414
IA(Q)	1482.93	1	1482.93	48.3909	0.000000
PCD(L)	354.60	1	354.60	11.5713	0.001310
DF * DP	35.39	1	35.39	1.1548	0.287599
DF * Conicity	46.54	1	46.54	1.5188	0.223446
DF * IA	847.14	1	847.14	27.6437	0.000003
DF * PCD	165.84	1	165.84	5.4118	0.024012
DP * Conicity	4.20	1	4.20	0.1371	0.712762
DP * IA	11.68	1	11.68	0.3811	0.539782
DP * PCD	0.00	1	0.00	0.0000	0.996184
Conicity * IA	52.79	1	52.79	1.7226	0.195231
Conicity * PCD	18.31	1	18.31	0.5974	0.443134
IA * PCD	88.76	1	88.76	2.8964	0.094868
Error	1562.89	32			
Total SS	19779.48	48			

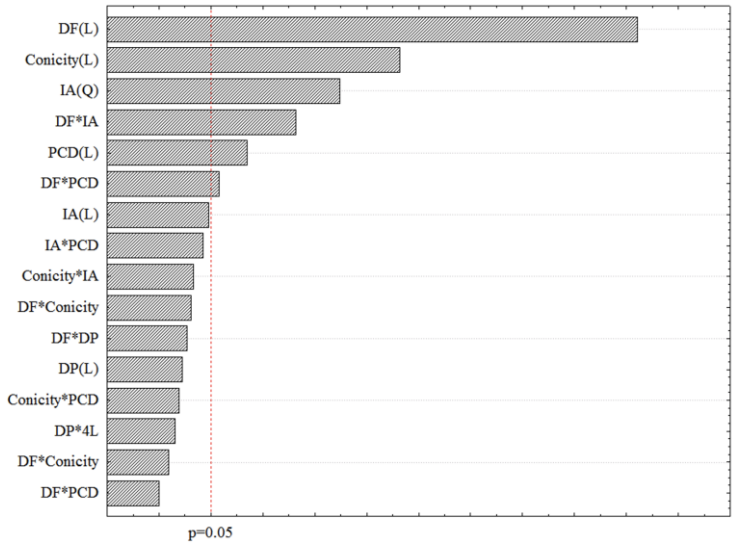

Fig. 8. Pareto chart of standardized effects for VVF, (L): Linear effect, (Q): Quadratic effect.

The CFD results for VVF, which were obtained for different experiment cases are summarized in Figs. 10-13. These results are also accordant with DOE result shown in Fig. 8. Figure 10 shows the effects of DF on vapor formation at a given design point. As seen, created VVF at the level E30 (58.14E-12 m^3) is higher than the level E85 (19.75E-12 m^3) due to higher saturation pressure, which leads to more vapor formation. Figure 11 displays effects of different Conicity on VVF. Since the Neg. level of Conicity leads to choking of flow and to decrease the separation region, it shows less vapor formation compared to Pos. level. Effects of different IA on vapor formation for a given point are shown in Fig. 12. As Fig. 12 shows, high level of IA results in larger separation region, and leads to more vapor formation compared to the low level. Finally, the effects of different levels of PCD on VVF is indicated in Fig. 13. PCD at Maximum level corresponds to the closer distribution of spray holes to flow field, which leads earlier separation and more vapor formation. Therefore, PCD at Maximum level shows more vapor formation (or cavitation) compared to Minimum level as can be seen in Fig. 13.

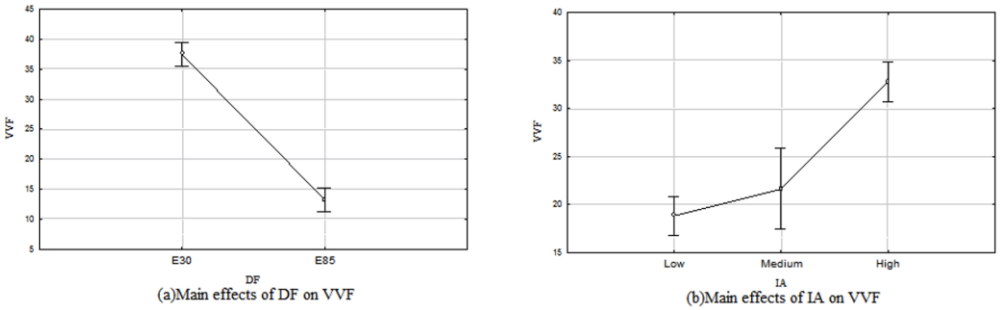

(a)Main effects of DF on VVF (b)Main effects of IA on VVF

(c)Main effects of Conicity on VVF (d)Main effects of PCD on VVF

Fig. 9. Main effect plots for VVF.

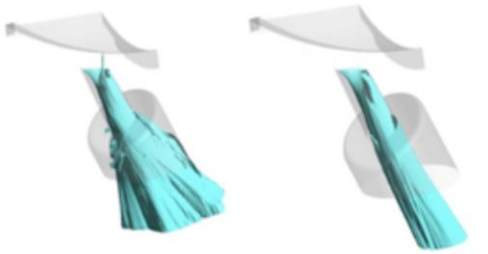

(a) Case 27 (b) Case 39

Fig. 10. Effects of different levels of DF on VVF, (a) DF = E30, VVF = 58.14E-12 (b) DF = E85, VVF = 19.75E-12.

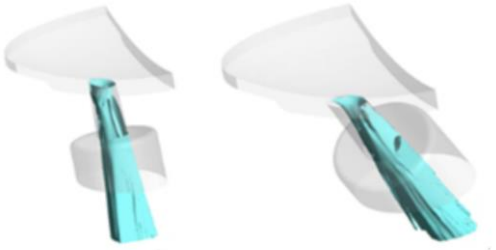

(a) Case 37 (b) Case 39

Fig. 12. Effects of different levels IA on VVF, (a) IA = Low, VVF = 15.37E-12 (b) IA = High, VVF = 18.07E-12.

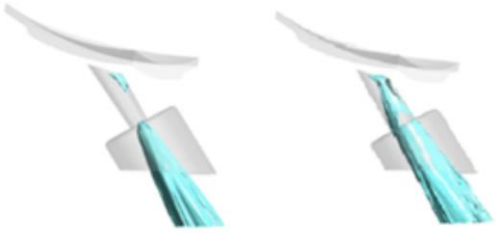

(a) Case 42 (b) Case 39

Fig. 11. Effects of different levels of Conicity on VVF, (a) Conicity = Neg., VVF = 6,18E-12 (b) Conicity = Pos., VVF = 18,07E-12.

(a) Case 37 (b) Case 43

Fig. 13. Effects of different PCD on VVF, (a) PCD = Minimum, VVF = 15.37E-12 (b) PCD = Maximum, VVF = 17.79E-12.

4.2 Effects of input parameters on spray angle (TauOut)

The ANOVA results on TauOut are summarized in Table 6. Similar to the previous subsection, the effects of the input parameters that are depicted in bold are statistically significant ($p < 0.05$) in 95% confidence level. As can be seen from Table 6, the linear effects of PCD, Conicity, IA, and the quadratic effect of IA significantly affect the response variable with p values 0.000034, 0.005942, 0.011655, and 0.002163 respectively. In contrast, the main effects of DifFules and DP are not statistically significant on TauOut. Also, there are no significant two-way interactions. The Pareto chart of standardized effects on TauOut is given in

Table 6 ANOVA results for TauOut

Source	Sum of Squares	Degree of freedom	Mean Square	F Value	*p*-value
DF(L)	29.503	1	29.5031	3.60038	0.063435
DP(L)	4.573	1	4.5725	0.55800	0.458495
Conicity(L)	67.550	1	67.5503	8.24342	0.005942
IA(L)	56.106	1	56.1058	6.84681	0.011655
IA(Q)	85.542	1	85.5423	10.43905	0.002163
PCD(L)	169.227	1	169.2272	20.65144	0.000034
DF by DP	0.301	1	0.3014	0.03679	0.848661
DF * Conicity	1.378	1	1.3783	0.16820	0.683438
DF * IA	11.314	1	11.3141	1.38071	0.245438
DF * PCD	1.267	1	1.2669	0.15460	0.695816
DP * Conicity	15.510	1	15.5095	1.89269	0.174911
DP * IA	0.132	1	0.1325	0.01617	0.899316
DP * PCD	0.262	1	0.2624	0.03202	0.858696
Conicity * IA	3.572	1	3.5718	0.43588	0.512088
Conicity * PCD	0.142	1	0.1417	0.01729	0.895906
IA * PCD	0.410	1	0.4099	0.05003	0.823912
Error	417.917	32			
Total SS	1225.373	48			

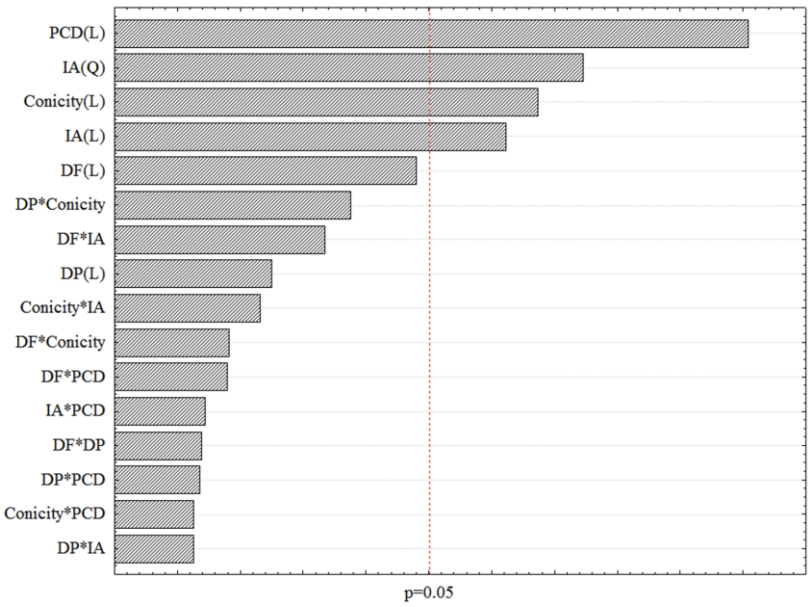

Fig. 14. Pareto chart of standardized effects for TauOut, (L): Linear effect, (Q): Quadratic effect.

Fig. 14. From Fig. 14, it can be seen that the most effective parameter on TauOut is PCD followed by the quadratic effect of IA and Conicity. Additionally, the main effect plots are presented in Fig. 15. From Fig. 15, TauOut values can be significantly decreased at the Low, Neg. and Minimum levels of IA, Conicity, and PCD respectively.

Lastly, Fig. 16 shows CFD results of TauOut achieved at different IA values for Cases 43 and 45. The calculated TauOut values at the high level of IA are larger than low level since higher IA leads to more separation and more vapor formation, which is directly proportional to the increase of Tau-angle. As can be also in Fig. 15, the Neg. level of Conicity and Minimum level of PCD cause to decrease of TauOut, since negative Conicity leads to choking of flow whereas minimum PCD results in orientation of holes more closer to the center. Therefore, TauOut shows a step-down trend in the case of Neg. level for Conicity and Minimum level of PCD.

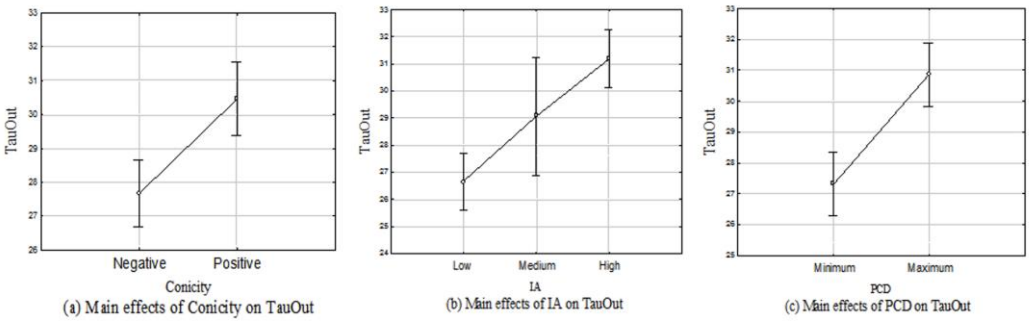

Fig. 15. Main effect plots for TauOut.

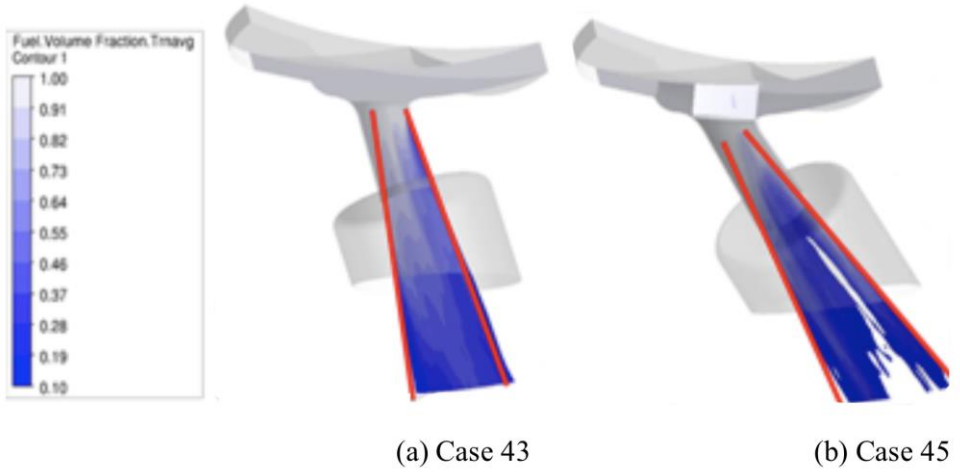

Fig. 16. Effects of different IA levels on TauOut, (a) IA = Low, TauOut = 28.24 (b) IA = High, TauOut = 31.42.

Table 7 ANOVA results for VSW1

Source	Sum of Squares	Degree of freedom	Mean Square	F Value	*p*-value
DF(L)	0.045169	1	0.045169	0.549265	0.462017
DP(L)	0.103479	1	0.103479	1.258334	0.267220
Conicity(L)	0.272227	1	0.272227	3.310348	0.074717
IA(L)	0.025561	1	0.025561	0.310833	0.579608
IA(Q)	0.366244	1	0.366244	4.453611	0.039752
PCD(L)	0.169030	1	0.169030	2.055443	0.157766
DF * DP	0.001875	1	0.001875	0.022804	0.880564
DF * Conicity	0.024102	1	0.024102	0.293084	0.590608
DF * IA	0.002192	1	0.002192	0.026651	0.870966
DF * PCD	0.105557	1	0.105557	1.283594	0.262530
DP * Conicity	0.021205	1	0.021205	0.257854	0.613787
DP * IA	0.010192	1	0.010192	0.123942	0.726249
DP * PCD	0.074912	1	0.074912	0.910945	0.344366
Conicity * IA	0.023460	1	0.023460	0.285282	0.595580
Conicity * PCD	0.000012	1	0.000012	0.000141	0.990556
IA * PCD	0.066995	1	0.066995	0.814679	0.370984
Error	4.193996	32			
Total SS	5.964116	48			

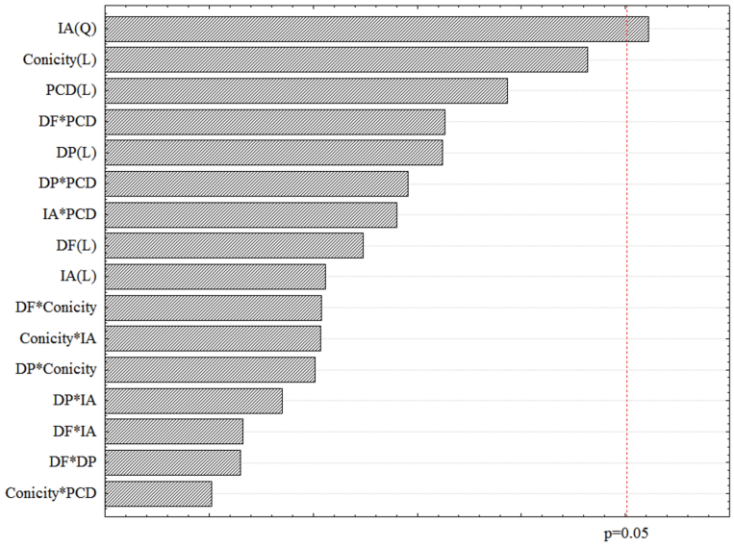

Fig. 17. Pareto chart of standardized effects for VSW1, (L): Linear effect, (Q): Quadratic effect.

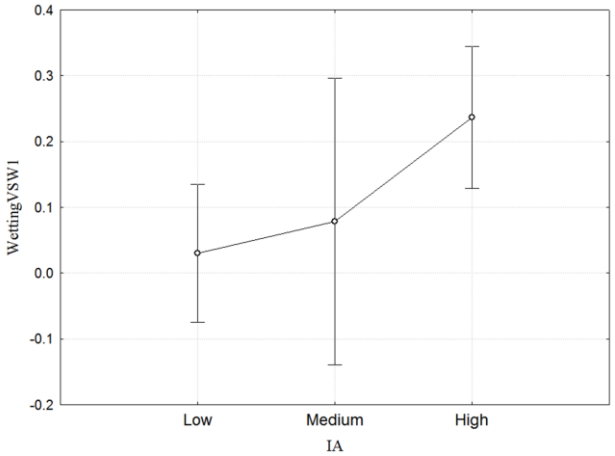

Fig. 18. Main effect plots for VSW1.

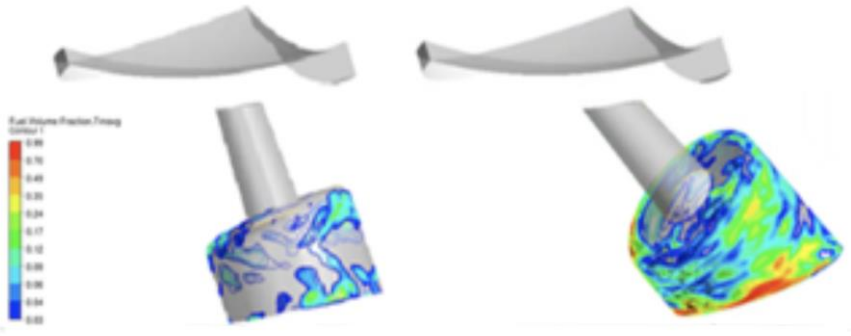

(a) Case 37 (b) Case 39

Fig. 19. Effects of different IA levels on VSW1, (a) IA = Low, VSW1 = 0.0924 (b) IA = High, VSW1 = 2.7590.

4.3 Effects of Input Parameters on Wall-Wetting

ANOVA results are tabulated in Table 7 for the response variable, VSW1. As aforementioned, VSW1 shows the amount of liquid fuel on the wall of injector's pre-hole in terms of percentage. From Table 7, it is clear that only the quadratic effect of IA

is statistically significant on VSW1. The effects of different levels of all other parameters such as DF, DP, Conicity, PCD, and two-way interactions are not statistically significant on VSW1. As can be seen from Table 7, the p-value for the quadratic effect of IA is 0.0397, which is below 0.05. Moreover, the Pareto chart of standardized effects on VSW1 and the main effects plot is given in Figs. 17-18. Similar to the results achieved from Table 7, the only important parameter is the IA as can be seen in Fig. 17.

Lastly, the effect of different IA levels on VSW1 value achieved at a given cases 37, and 39 are illustrated in Fig. 19. As can be seen from Fig. 19, IA at High level causes more separation of flow fields and extension of angle in the outlet side of the spray hole. Therefore, High level of IA (VSW1 = 2.7590) creates much more wall pre-hole wetting compared to Low level of IA (VSW1 = 0.0924).

5. CONCLUSION

In this study, the parameter and design analysis in the valve-seat region of direct gasoline injection (GDI) injector have been carried out using Computational Fluid Dynamics (CFD) and Design of Experiments (DOE). In DOE studies, the significance of both the main effects and interaction effects of injection pressure, fuel type, I-angle, conicity and pitch circle diameter parameters are analyzed on various response variables. It is found that PCD is the most significant input parameter on spray (Tau) angle, whereas IA is the determinant factor for wall-wetting. Additionally, fuel type is found to be the most significant factor on the vapor/cavitation formation due to physical properties of fuels. Those results can be used in the design phase of valve-seat in GDI injector to increase the atomization (which is directly related vapor formation and spray angle) and decrease the emission (which is also related excessive wall-wetting).

Further studies in the DOE side may cover implementing different regression models or response surface methodologies to effectively determine the relation between design and response parameters. Also, the presented results will be validated and verified with test results in the future as an extension of this work.

ACKNOWLEDGMENTS

This research is a collaboration between industry (Robert Bosch Sanayi ve Ticaret A.Ş.) and Uludağ University which is supported by Scientific and Technological Research Council of Turkey - TÜBİTAK (No: 3161154). The authors would like to thank the editor, anonymous referees, and Prof. Alper Ozalp for their helpful comments and suggestions on improving the presentation of this paper.

REFERENCES

ANSYS, C., (2015). "Release 16.2". *Canonsburg (PA): ANSYS Inc*, 15317.

Antony, J. (2014). *Design of Experiments for Engineers and Scientists.* Second ed. Elsevier.

Bicer, B., A.,Tanaka, T., Fukuda and A. Sou (2013). Numerical simulation of cavitation phenomena in diesel injector nozzles, *16th Annual Conference ILASS-ASIA*, Nagasaki-Japan, pp. 58-65.

Bicer, B. (2015). *Numerical Simulation of Cavitation Phenomena inside Fuel Injector Nozzles*. Ph. D. thesis, Kobe University, Japan.

Bicer, B. and Sou, A., (2015). Numerical models for simulation of cavitation in diesel injector nozzles. *Atomization and Sprays* 25.

Biçer, B. and Sou, A., (2016). Application of the improved cavitation model to turbulent cavitating flow in fuel injector nozzle. *Applied Mathematical Modelling* 40(7-8), 4712-4726.

Chapela, S., J. Porteiro, M. Gómez, D. Patiño and J. Míguez (2018). Comprehensive CFD modeling of the ash deposition in a biomass packed bed burner. *Fuel* 234, 1099-1122.

Chaves, H., M. Knapp, A. Kubitzek, F. Obermeier and T. Schneider (1995). Experimental study of cavitation in the nozzle hole of diesel injectors using transparent nozzles. *SAE Transactions* 645-657.

Chen, L., Z. Liu, P. Sun and W. Huo (2015). Formulation of a fuel spray SMD model at atmospheric pressure using Design of Experiments (DoE). *Fuel* 153, 355-360.

Ferrari, A. (2010). Modelling approaches to acoustic cavitation in transmission pipelines. *International Journal of Heat and Mass Transfer* 53(19-20), 4193-4203.

Gong, C. and R. Baar (2017). Study of the influence of low needle lifts process on the internal flow and spray characteristics in Diesel injection nozzle. *17. Internationales Stuttgarter Symposium*. Springer, Stuttgart, Germany, pp. 989-1011.

He, Z., G. Guo, X. Tao, W. Zhong, X. Leng and Q. Wang (2016). Study of the effect of nozzle hole shape on internal flow and spray characteristics. *International Communications in Heat and Mass Transfer* 71, 1-8.

He, Z. and E. M. Dass (2018). Correlation of design parameters with performance for electrostatic precipitator. Part II. Design of experiment based on 3D FEM simulation. *Applied Mathematical Modelling* 57, 656-669.

Henn, A. (2012). *CFD-Simulation der Düsenausströmung und Wandbenetzung in einem Mehrloch-Injektor*. MSc Thesis, Stuttgart University

Hiroyasu, H. (1991). Break-up length of a liquid jet and internal flow in a nozzle, *Proc. 5th. ICLASS*, Paper Id:91, Gaithersburg, MS, USA, 275-282.

Jin, H. and A. Untaroiu (2018). Elliptical Shape Hole-Pattern Seals Performance Evaluation Using Design of Experiments Technique. *Journal of Fluids Engineering* 140, 071101.

Kear, M., B. Evans, R. Ellis and S. Rolland (2016). Computational aerodynamic optimisation of vertical axis wind turbine blades. *Applied Mathematical Modelling* 40(2), 1038-1051.

Lee, S., Y. Park J. and Kim (2018). An evaluation of factors influencing drag coefficient in double-deck tunnels by CFD simulations using factorial design method. *Journal of Wind Engineering and Industrial Aerodynamics* 180, 156-167.

Menter, F. R. (1994). Two-equation eddy-viscosity turbulence models for engineering applications. *AIAA journal* 32(8), 1598-1605.

Montgomery, D. C. (2017). *Design and analysis of experiments*. John wiley & Sons.

Pierrat, D., L. Gros, G. Pintrand, B. Le Fur and P. Gyomlai (2008). Experimental and numerical investigations of leading edge cavitation in a helico-centrifugal pump, *The 12th International Symposium of Transport Phenomena and Dynamics on Rotating Machinery*, Honolulu, HI, USA, 17-22.

Prosperetti, A. (1982). A generalization of the Rayleigh–Plesset equation of bubble dynamics. *The Physics of Fluids* 25(3), 409-410.

Sou, A., S. Hosokawa and A. Tomiyama (2007). Effects of cavitation in a nozzle on liquid jet atomization. *International journal of heat and mass transfer* 50(17-18), 3575-3582.

Wang, Z., Y. Wang and M. Zhuang (2018). Improvement of the aerodynamic performance of vertical axis wind turbines with leading-edge serrations and helical blades using CFD and Taguchi method. *Energy Conversion and Management* 177, 107-121.

WHO (2003). *Health aspects of air pollution with particulate matter, ozone and nitrogen dioxide: report on a World Health Organization working group*, Bonn, Germany 13-15 January 2003.

Xu, M., Y. Cui and K. Deng (2016). One-dimensional model on liquid-phase fuel penetration in diesel sprays. *Journal of the Energy Institute* 89(1), 138-149.

Yang, M., D. Yu, M. Liu, L. Zheng, X. Zheng, Y. Wei, F. Wang and Y. Fan (2017). Optimization of MBR hydrodynamics for cake layer fouling control through CFD simulation and RSM design. *Bioresource technology* 227, 102-111.

Yoon, J. and J. Lee (2018). Parameter analysis and design for the hovering thrust of a quad-rotor air vehicle using CFD and design of experiment. *Journal of Mechanical Science and Technology* 32(2), 781-791.

Zhang, D., D. Pan, W. Shi, S. Wu and P. Shao (2013). Study on Tip Leakage Vortex in an Axial Flow Pump Based on Modified Shear Stress Transport K-Omega Turbulence Model. *Thermal Science* 17(5), 1551-1555.

Zhang, Y., G. Yu, M. A. H. Siddhu, A. Masroor, M. F. Ali, A. A. Abdeltawab and X. Chen (2017). Effect of impeller on sinking and floating behavior of suspending particle materials in stirred tank: A computational fluid dynamics and factorial design study. *Advanced Powder Technology* 28(4), 1159-1169.